RESEARCH ARTICLE

Improved fuzzy sliding mode control in flexible manipulator actuated by PMAs

Fang Li[1], Zheng Zhang[2], Yang Wu[2], Yining Chen[2], Kai Liu[2,*] and Jiafeng Yao[2]

[1]Sanjiang University, No.10, Longxin Road, Yuhuatai District, Nanjing City, Nanjing 210016, China and [2]Nanjing University of Aeronautics and Astronautics, No. 29, Yu Dao Street, Qin Huai District, Nanjing City, Nanjing 210016, China
*Corresponding author. E-mail: liukai@nuaa.edu.cn

Abstract
Pneumatic muscle actuator (PMA) similar to biological muscle is a new type of pneumatic actuator. The flexible manipulator based on PMAs was constructed to simulate the actual movement of the human upper arm. Considering the model errors and external disturbances, the fuzzing sliding mode control based on the saturation function was proposed. Compared with other fuzzy control methods, fuzzy control and saturation function are used to adjust the robust terms to improve the tracking accuracy and reduce the high-frequency chattering.

1. Introduction

Pneumatic muscle actuator (PMA) and biological muscle characteristics are similar. PMA perform energy conversion, distribution, and control with gas as medium, which is not only low cost, convenient maintenance, environmentally friendly but also simple structure, large output power/weight ratio, good flexibility [1]. PMA is also one of the typical representatives of the new type of pneumatic components and has been applied to the lower-limb rehabilitation [2], arms orthotics [3], and imitating the human neck [4]. In the future, PMA will have a broad application prospect in the fields of medical treatment, bionics, and military and the research on pneumatic muscles will also become a new hotspot in the field of humanoid robots [5].

Considering the limitations of its own structure, including the elasticity of the rubber hose, the friction between the fibers, and the change of environmental temperature, PMA's working process is nonlinear [6]. Besides, the actual mechanical structure processing and assembly deviation, uneven mass distribution, friction and other uncertain factors, some errors exist between the flexible manipulator actual control system and the ideal dynamic model, which brings great difficulty to the motion control of PMA.

Many studies have been carried out to achieve precise trajectory tracking control of PMA. Zhu et al. proposed a discontinuous projection-based adaptive robust control strategy to compensate for both the parametric uncertainties and uncertain nonlinearities of a three-pneumatic-muscles-driven parallel manipulator to achieve precise posture trajectory tracking control [7]. Ba et al. proposed an indirect robust nonlinear controller for position-tracking control of a pneumatic artificial muscle testing system [8], and the method is confirmed with respect to transient response, steady-state behavior, and loading effect. Ahn et al. proposed an adaptive recurrent neural networks (ARNN) controller suitable for real-time manipulator control applications to controlling the joint angle position of the highly nonlinear pneumatic artificial muscle manipulator in real-time [9]. Amato et al. established an optimal control problem considering both robust constraints and disturbance suppression requirements, after representing the tracking error system as a bilinear system with nonlinear perturbation terms [10].
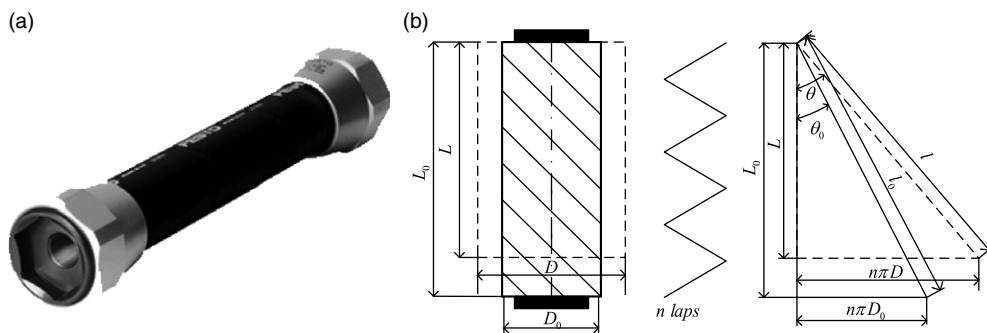
Figure 1. *FESTO pneumatic tendon. (a) Physical product. (b) Structure diagram.*

Xie et al. proposed a modified Prandtl–Ishlinskii (MPI) model for the asymmetric hysteresis characterization and compensation of the PMA using fast switching valves and its effectiveness on compensating the asymmetric length/pressure hysteresis of the PMA [11]. However, high-frequency shaking caused by discontinuous switching of sliding mode may lead to instability of system, the artificial neural network is only valid for the description of single-loop hysteresis, which cannot be directly used for the modeling of the multivalued hysteresis loops, and the classical PI model is unable to describe asymmetric hysteresis loops because of the symmetric property of linear play operators [12].

Compared with above control strategies, the PI robust sliding mode control strategy is adopted to reduce the influence of modeling errors and external disturbance factors. Besides the fuzzy sliding mode control strategy based on the saturation function is adopted to further improve the response speed of the system and suppress the high-frequency chattering of the sliding mode control.

The paper is organized as follows. Section 2 analyzes the structure of PMA and gives the mathematical model of PMA during tensile process. Section 3 presents the improvement and stability of proposed algorithm, then we verify the proposed algorithm through simulation experiment. Section 4 shows the experimental platform and the results of the trajectory tracking experiment. In Section 5, we draw the conclusions of the paper.

2. PMA

2.1. Analyze of PMA's structure

The PMA used in the experiment is the pneumatic tendon developed by FESTO company, as shown in Fig. 1. The PMA is mainly composed of an internal rubber tube, a peripheral braided sleeve, and a fastening head at both ends. The rubber hose has good elasticity while the braid sleeve has great rigidity. When the rubber hose is pressurized with gas, its radial expansion and axial shortening will generate external tension, so as to convert the gas pressure energy into mechanical energy and drive the load.

During the process of inflatable contraction, the pneumatic muscle expands radially and contracts axially at the same time. It can be concluded that the length of a single fiber l stays constant [13], as shown in Fig. 1(b), because of the very large stiffness of the fiber sheath. Thus, the relationship among the geometrical parameters of fiber length, muscle length, and radial circumference can be obtained as follows:

$$\begin{cases} L_0 = l\cos\theta_0 \\ n\pi D_0 = l\sin\theta_0 \end{cases} \Rightarrow \begin{cases} L = l\cos\theta \\ n\pi D = l\sin\theta \end{cases} \tag{1}$$

where let L_0 and L be the initial length and real-time length of the pneumatic muscle respectively, D_0 and D be the initial diameter and real-time diameter of the aerodynamic muscle section, l be the length
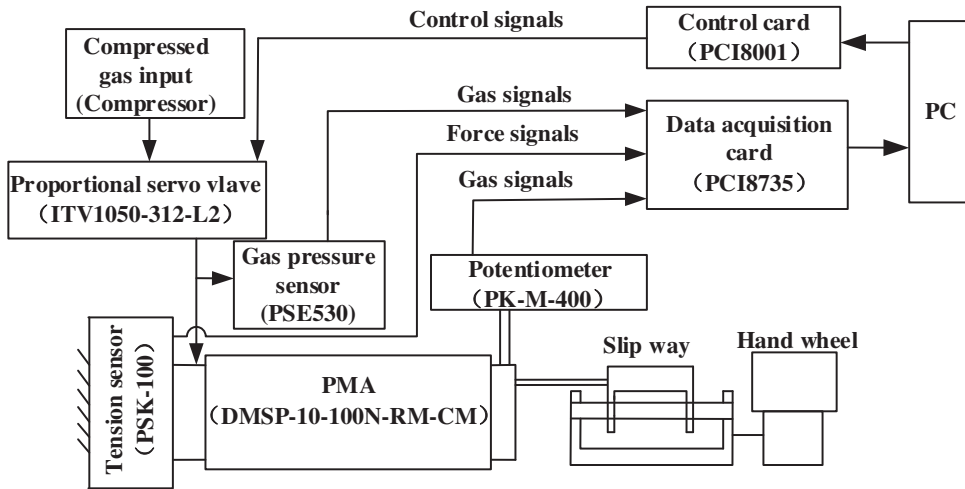
Figure 2. *Static test schematic diagram of single PMA.*

of a single fiber of pneumatic muscle, n be the number of winding cycles of a single fiber, and θ_0 and θ be the angle between the fiber and the axis at the initial moment and in real time, respectively.

2.2. The mathematical model of PMA's tensile

In order to achieve accurate control of PMA, the first step is to establish the mathematical model, namely, the mathematical model between the load tension F, the shrinking percentage ε, and the charging pressure P. In this paper, a static examine platform (as shown in Fig. 2) is used for static test of a single pneumatic muscle, which can be divided into contraction test and tensile test. During the experiment, contraction test refers to continuously inflating air to make the pneumatic muscle contract from the original length to the limit position, while tensile test refers to continuously deflating air to restore the original length from the limit position of contraction.

MATLAB curve fitting toolbox was used to fit the test data of 110 mm pneumatic muscle in the process of contraction and stretching, the fitting degree was around 0.99, and the mathematical models obtained are as follows:

$$
\begin{cases}
\Delta P < 0: \ F = P \left(0.0305\varepsilon^3 - 1.134\varepsilon^2 - 14.72\varepsilon + 819.9\right) + \\
\qquad \left(0.00257\varepsilon^4 - 0.1758\varepsilon^3 + 4.263\varepsilon^2 - 42.54\varepsilon - 0.28\right) \\
\Delta P \geq 0: \ F = P \left(0.0305\varepsilon^3 - 1.134\varepsilon^2 - 14.72\varepsilon + 819.9\right) + \\
\qquad \left(0.00257\varepsilon^4 - 0.1758\varepsilon^3 + 4.263\varepsilon^2 - 42.54\varepsilon + 0.21\right)
\end{cases} \tag{2}
$$

3. Fuzzy sliding mode control based on saturation function

3.1. PI robust sliding mode control

Sliding mode control is a kind of variable structure control strategy. The control system structure is not fixed but constantly changes with time, which is essentially different from the conventional control strategy. During actual motion process of flexible manipulator, many uncertainties exist in the dynamic

model, where $M(q)$, $C(q, \dot{q})$ and $G(q)$ are usually inaccurate, which can be expressed as

$$\begin{cases} M(q) = M_0(q) + E_M \\ C(q, \dot{q}) = C_0(q, \dot{q}) + E_c \\ G(q) = G_0(q) + E_G \end{cases} \tag{3}$$

where let E_M, E_c, and E_G be the modeling errors of $M(q), C(q, \dot{q})$, and $G(q)$, respectively, $M_0(q), C_0(q, \dot{q})$, and $G_0(q)$ be the estimated values of the inertia coefficient, the Coriolis force, the centrifugal force term, and the gravity term, respectively, which is so-called nominal model.

Noted $q_d(t)$ as the ideal angle signal of the joint and $q(t)$ as the actual angle signal. So, the tracking error of the two joint angles is defined as

$$e(t) = q_d(t) - q(t) \tag{4}$$

The sliding mode function is defined as follows (where $\Lambda > 0$):

$$r = \dot{e} + \Lambda e \tag{5}$$

Noted $\dot{q}_r = r(t) + \dot{q}(t)$, then $\ddot{q}_r = \dot{r}(t) + \ddot{q}(t)$, $\dot{q}_r = \dot{q}_d + \Lambda e$, $\ddot{q}_r = \ddot{q}_d + \Lambda \dot{e}$. So, the following can be obtained from the dynamic model of flexible manipulator:

$$\begin{aligned} \tau &= M(q)\ddot{q} + C(q, \dot{q})\dot{q} + G(q) + \tau_d \\ &= M_0(q)\ddot{q}_r + C_0(q, \dot{q})\dot{q}_r + G_0(q) - M(q)\dot{r} - C(q, \dot{q})r + E' + \tau_d \end{aligned} \tag{6}$$

where $E' = E_M\ddot{q}_r + E_c\dot{q}_r + E_G$.

The control rate of PI robust sliding mode control is designed as follows:

$$\tau = \tau_m + K_p r + K_i \int r dt + \tau_r \tag{7}$$

where $K_p > 0$, $K_i > 0$, and τ_m are torque vector control based on the name of the flexible manipulator model, $K_p r + K_i \int r dt$ is PI sliding mode surface, and τ_r is robust term.

According to (7), the following can be deduced:

$$\begin{cases} \tau_m = M_0(q)\ddot{q}_r + C_0(q, \dot{q})\dot{q}_r + G_0(q) \\ \tau_r = K_r sgn(r) \end{cases} ; \tag{8}$$

where $K_r = diag[k_{rii}]$, $k_{rii} \geq |E_i|$, $i = 1, 2, E = E' + \tau_d$.

Further, according to (6) and (8), Eq. (9) can be deduced:

$$\begin{aligned} &M_0(q)\ddot{q}_r + C_0(q, \dot{q})\dot{q}_r + G_0(q) - M(q)\dot{r} - C(q, \dot{q})r + E' + \tau_d \\ &= M_0(q)\ddot{q}_r + C_0(q, \dot{q})\dot{q}_r + G_0(q) + K_p r + K_i \int r dt + K_r sgn(r) \end{aligned} \tag{9}$$

Simplified both two sides of the above formula, Eq. (10) can be deduced:

$$M(q)\dot{r} + C(q, \dot{q})r_r + K_i \int r dt = -K_p r - K_r sgn(r) + E \tag{10}$$

3.2. Stability of the PI robust sliding mode control

Lyapunov function based on integral type is designed as follows:

$$V = \frac{1}{2}r^T M r + \frac{1}{2}\left(\int r d\tau\right)^T K_i \left(\int r d\tau\right) \tag{11}$$

Obviously, V is positive definite, then:

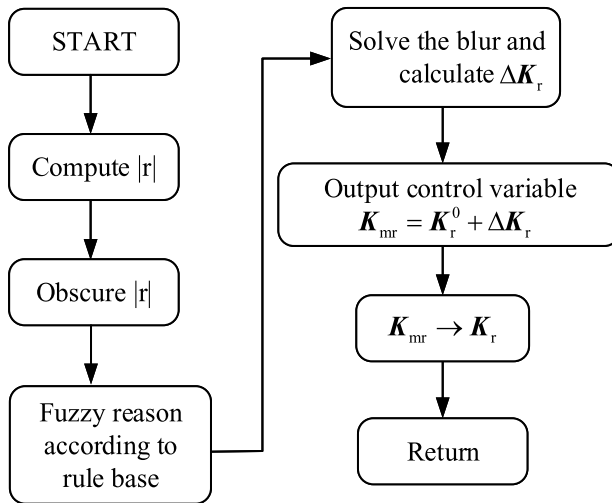$$\dot{V} = r^T \left(M\dot{r} + \frac{1}{2}\dot{M}r + K_i \int r d\tau\right) \tag{12}$$
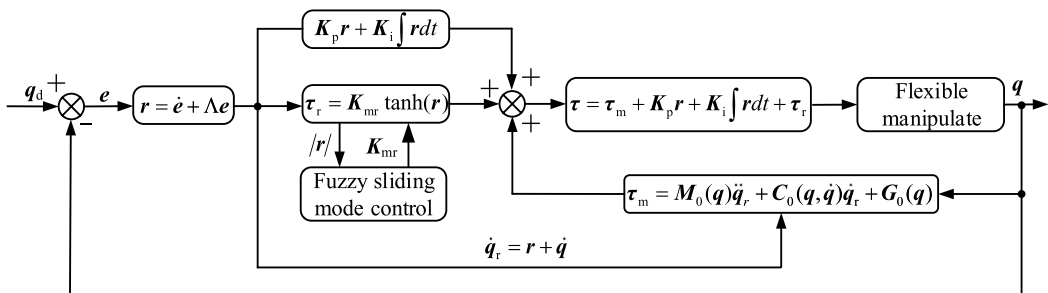
Figure 3. *Flow chart of the fuzzy classifier.*

Figure 4. *Fuzzy sliding mode control.*

Considering Skew symmetry of kinetic equation, $r^{\mathrm{T}}(M - 2C)r = 0$, then:

$$\dot{V} = r^{\mathrm{T}}\left(Mr + Cr + K_i \int rd\tau\right) \tag{13}$$

Substituting Eq. (10) into Eq. (13):

$$\dot{V} = -r^{\mathrm{T}}K_p r - r^{\mathrm{T}}K_r sgn(r) + r^{\mathrm{T}}E = -r^{\mathrm{T}}K_p r - \sum_{i=1}^{2} K_{rii}|r|_i + r^{\mathrm{T}}E \tag{14}$$

where $K_{rii} \geq |E_i|$, so $\dot{V} \leq -r^{\mathrm{T}}K_p r \leq 0$.

Because $\dot{V}$ is a negative definite matrix, the control system is stable.

3.3. Improvement of the sliding mode control

The PI robust sliding mode control has its inherent shortcoming that is the phenomenon high-frequency chattering, which can only be reduced, not eliminated. Therefore, a fuzzy sliding mode control strategy based on the saturation function is proposed to improve the robustness of PI robust sliding mode control. Compared with the method of eliminating high-frequency chattering directly by using saturated function [14], we use fuzzy control strategy to modify the robust term coefficient, so as to ensure the rapidity and robustness of the sliding mode control.
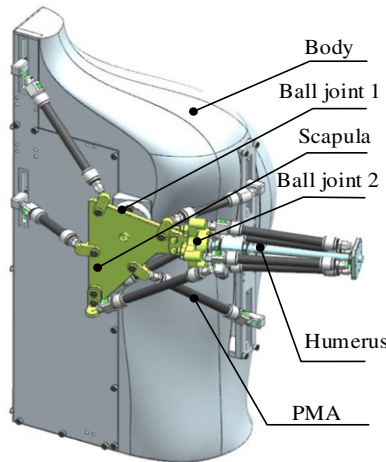
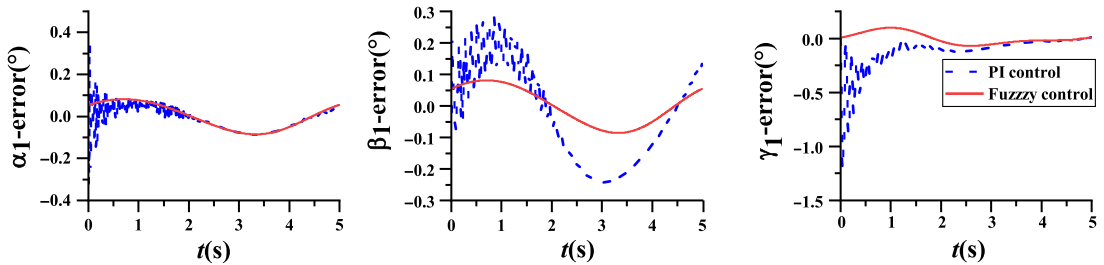**Figure 5.** *Simulation model of flexible manipulator.*

Figure 6. *Tracking degree error of α_1, β_1, and γ_1 at scapula joint.*
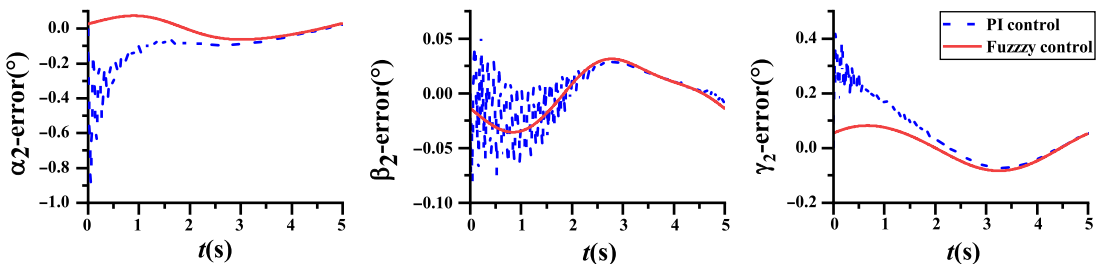
Figure 7. *Tracking degree error of α_2, β_2, and γ_2 at humeral joint.*

From (8), the robust term of PI robust sliding mode control is as follows:

$$\tau_r = K_r sgn(r) \tag{15}$$

When $r \to 0$, $K_r sgn(r)$ does not approach zero, and the system state will move in and out frequently on both sides of the sliding switching surface, which caused chattering of the control system, and the strength of chattering depends on the size of the robust term coefficient K_r. In order to effectively reduce chattering, a fuzzy controller is adopted to adjust the size of the robust term coefficient K_r. The flow chart of the fuzzy classifier is shown in Fig. 3.

In the actual control process, because the system error and external disturbance cannot be predicted accurately, angle tracking error e is bound to be generated in the two joint platforms, and the sliding mode surface r is a function of e. Therefore, according to the absolute value of r, the system error and

Table I. *Simulation error range of scapula joint position tracking.*

Joint angles	α1	β1	γ1
PI control	−0.530–0.602	−0.290–0.183	−0.616–0.584
Fuzzy control	−0.255–0.275	−0.208–0.154	−0.384–0.209
△	−53.2%	−23.5%	−50.6%

Table II. *Simulation error range of humeral joint location tracking.*

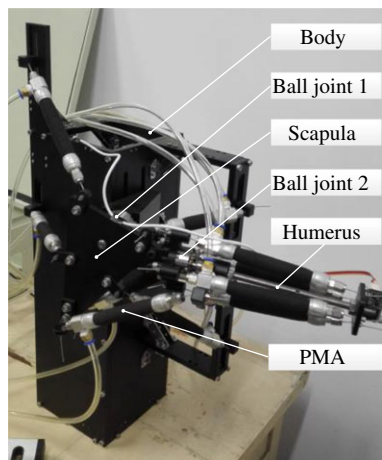| Joint angles	α2	β2	γ2
PI control	−0.500–0.901	−0.467–0.477	−0.338–0.554
Fuzzy control	−0.486–0.260	−0.348–0.398	−0.199–0.204
△	−46.8%	−21.0%	−54.8%

Figure 8. *Actual flexible manipulator.*

external disturbance can be estimated to adjust the coefficient K_r of robust term adaptively. The r as absolute value of the sliding mode surface is taken as the input variable of the fuzzy controller, and the output variable of the fuzzy controller is the variation of the robust term coefficient, and its adaptive adjustment formula is as follows:

$$K_{mr} = K_r^0 + \Delta K_r \quad (16)$$

where K_{mr} is the robust term coefficient solved by the fuzzy controller, and K_r^0 is the initial value of the robust term coefficient.

The switching process of sign function $sgn(r)$ is not continuous and smooth, which is another main reason for the high-frequency chattering phenomenon of the system. The saturation function method is used to redesign the function of the robust term, which takes the hyperbolic tangent function instead of the sign function to make the output smooth and bounded. The concrete expression of hyperbolic tangent function is as follows:

$$\tanh(r) = \frac{exp(r) - exp(-r)}{exp(r) + exp(-r)} \quad (17)$$

The concrete expression of the modified fuzzy robust term is
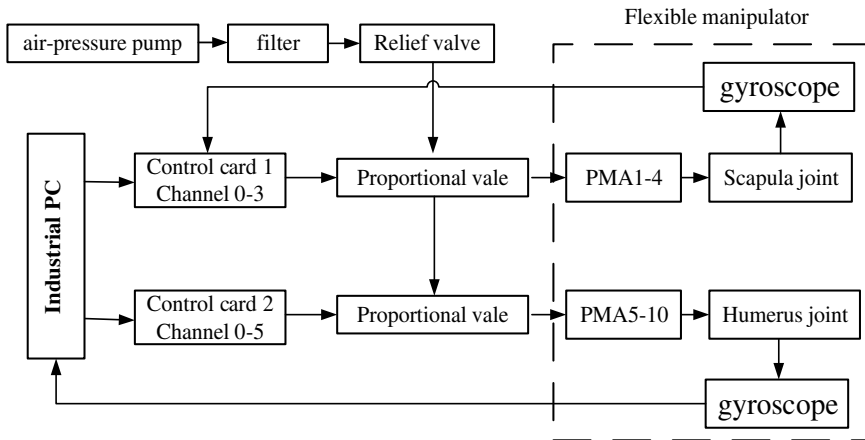
$$\tau_r = K_{mr}\tanh(r) \quad (18)$$

Figure 9. *Hardware block diagram of the flexible manipulator test platform.*
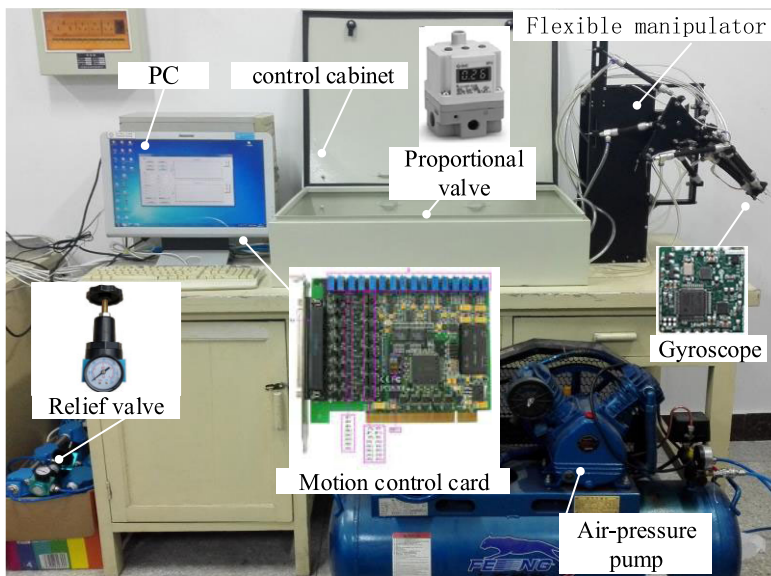

Figure 10. *Schematic diagram of the test platform.*

In summary, the control block diagram of the fuzzy sliding mode control strategy based on the saturation function is shown in Fig. 4, and its control law is

$$\tau = \tau_m + K_p r + K_i \int r dt + K_{mr} \tanh(r) \tag{19}$$

3.4. Simulation and verification

The manipulator arm is driven by two parallel joints, the scapula joint and the humerus joint. During the process of co-simulation, according to the desired trajectory, two joints are simultaneously controlled to simulate the motion, which can greatly reflect the interaction of the whole flexible manipulator under the actual motion. The structure of the flexible manipulator is shown in Fig. 5 as following:
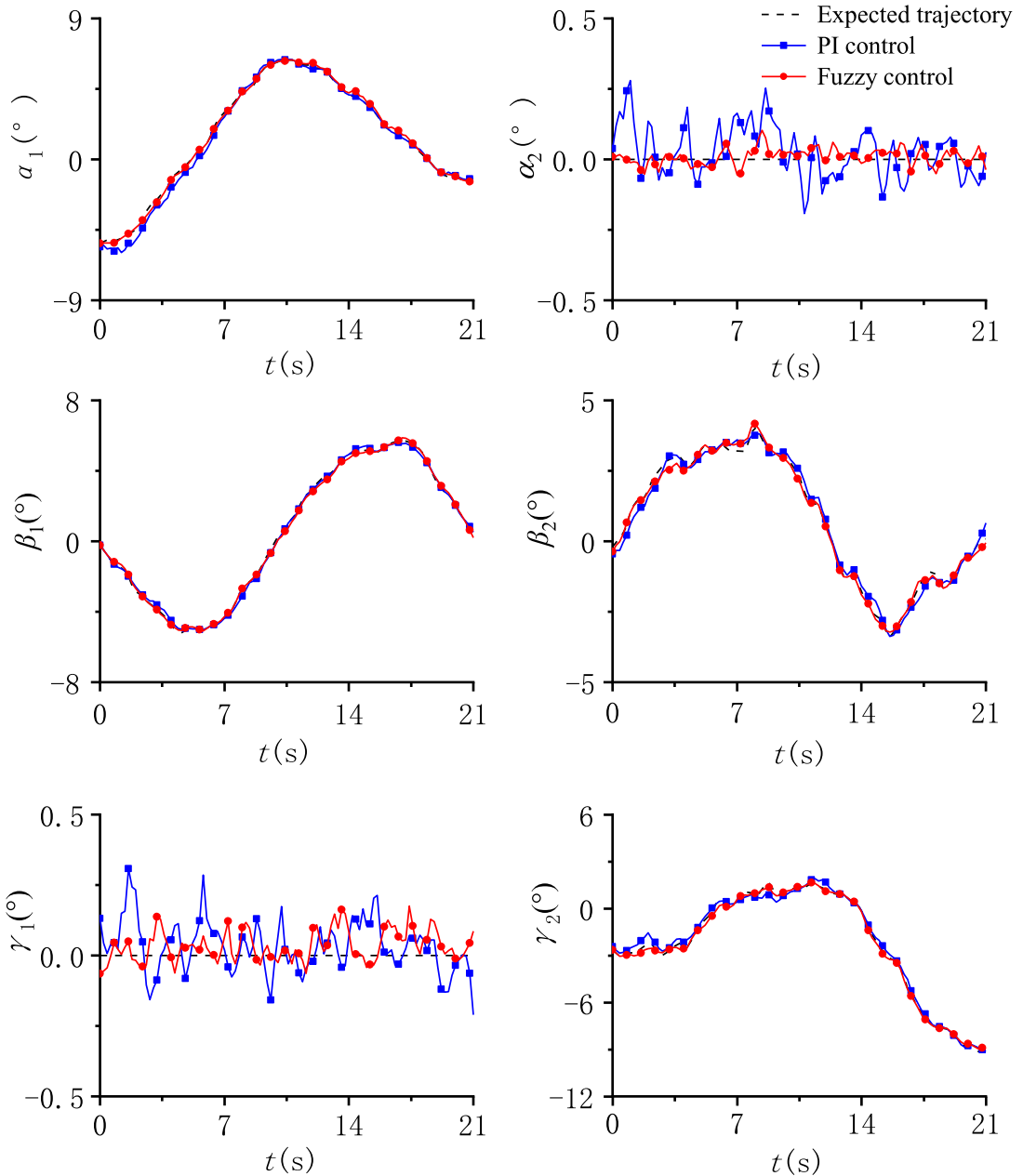
Figure 11. *Experimental curves of joints' angle.*

Setting the desired trajectory of scapula and humerus joints as follows:

$$\alpha = 10 \cdot \sin\left(\frac{2\pi}{5}t\right), \ \beta = 10 \cdot \sin\left(\frac{2\pi}{5}t\right), \ \gamma = 10 \cdot \sin\left(\frac{2\pi}{5}t\right) \quad [\text{deg}] \quad (20)$$

In the simulation of flexible manipulator, setting motion as $10 \cdot \sin(2\pi t/5)$ for each direction of shoulder blade joint and humerus joints, then we analyze the simulation results, respectively, under the nominal model PI robust sliding mode control and fuzzy sliding mode control based on saturated function.

Table III. *Experimental error range of scapula joint position tracking.*

Joint angles	α1	β1	γ1
PI control	−0.927–0.289	−0.444–0.310	−0.210–0.308
Fuzzy control	−0.364–0.333	−0.273–0.227	−0.065–0.176
△	−42.9%	−33.7%	−53.5%

Table IV. *Experimental error range of humerus joint position tracking.*

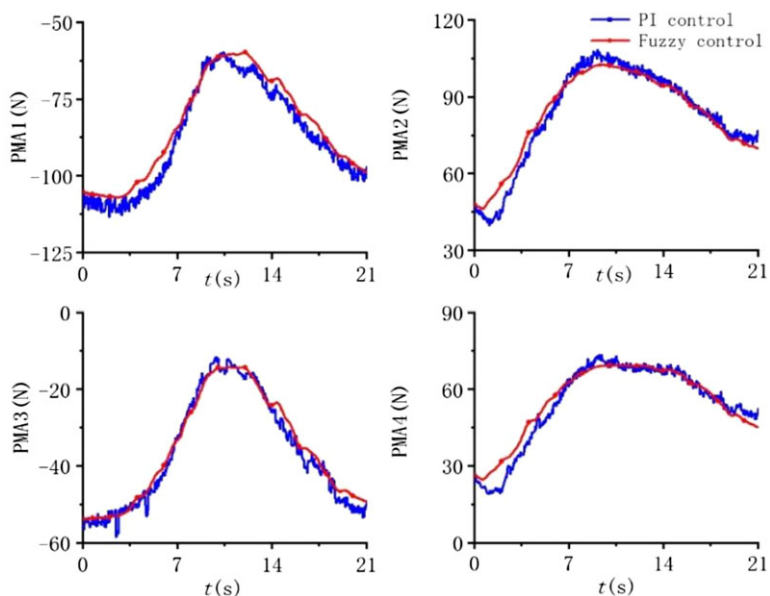| Joint angles	α2	β2	γ2
PI control	−0.182–0.280	−0.477–0.564	−0.745–0.667
Fuzzy control	−0.106–0.124	−0.378–0.377	−0.431–0.263
△	−50.2%	−27.5%	−50.8%

Figure 12. *Control force of each PMA of scapula joint.*

For scapula joint, the initial parameters of the two sliding mode controls are as follows:

$$K_{p1} = diag[3750, 3750, 3750], \ K_{i1} = diag[35, 35, 35], \ K_{r1} = diag[30, 30, 30].$$

For humerus joint, the initial parameters of the two sliding mode controls are

$$K_{p2} = diag[3200, 3200, 3200], \ K_{i2} = diag[20, 20, 20], \ K_{r2} = diag[15, 15, 15].$$

Through the cosimulation by MATLAB and ADAMS, position tracking simulation graphics of the scapula and humerus joints, respectively, under two sliding mode control strategies are shown as Figs. 6 and 7.

During the overall process of simulation, the robust parameters of PI robust sliding mode control are fixed. However, the interference of the two joints' movement can make the system parameters change with the status of movement, and the changes are unknown that have huge influence on the control process probably. The specific control effect is shown in Table I and Table II. The tracking error range of fuzzy sliding mode was reduced. It has better dynamic quality such as high control accuracy and well adaptability.
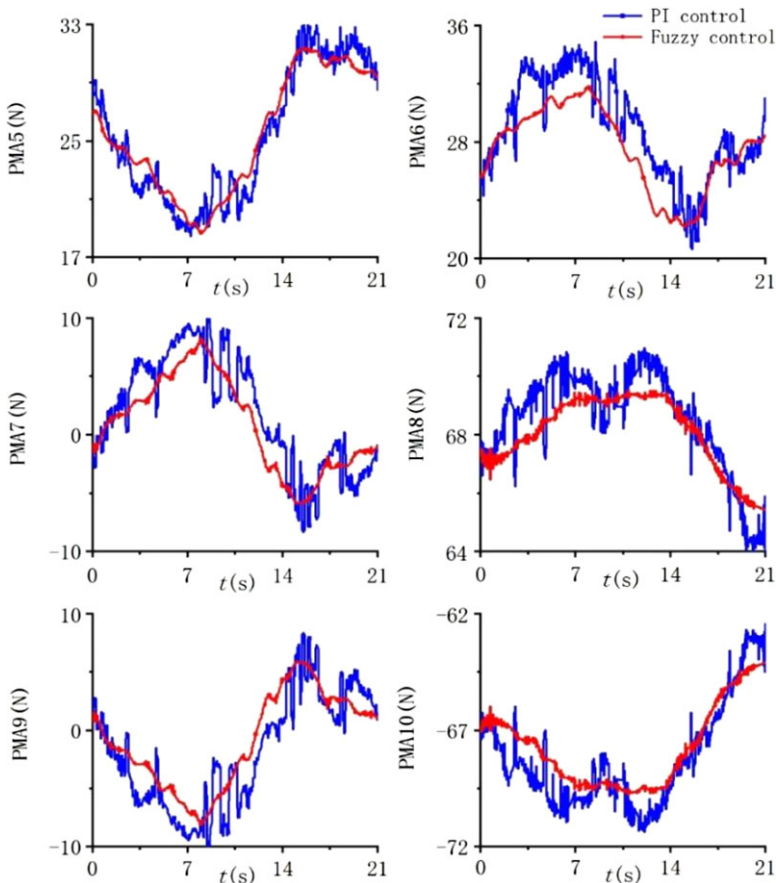
Figure 13. *Control force of each PMA of humerus joint.*

4. Experimental verification of the flexible manipulator

4.1. Design of flexible manipulator test platform

In this paper, the flexible manipulator is a series-parallel mechanical structure driven by multiple pneumatic muscles, which is formed by a parallel platform of scapula joint and a parallel platform of humerus joint in series, and is jointly driven by 10 pneumatic muscles in different positions. The actual flexible manipulator is shown in Fig. 8.

The scapula joint is composed of two pneumatic muscles titled DMSP-10N-110-RM-CM and two pneumatic muscles titled DMSP-10N- 55-RM-CM. The humerus joint is driven by six pneumatic muscles titled DMSP-10N-110-RM-CM. The hardware design of the flexible manipulator test platform is mainly composed of industrial PC, filter, relief valve, proportional valve, air-pressure pump, PCI D/A controller, gyroscope, and so on. The hardware block diagram of the flexible manipulator test platform and the physical map of the test platform are shown in Figs. 9 and 10, respectively:

According to the test requirements of the flexible manipulator control system, the LABVIEW library functions provided by PCI8201 and gyroscope were called in the NI LabVIEW2013 environment, and the MATLAB script was used for complex numerical calculation. According to the above two control strategies, we controlled the movement of the executive end of flexible manipulator in order to carry out arc trajectory tracking control experiment. First, an appropriate projection surface is selected, and then the executive end of the flexible manipulator moves in an arc on the projection surface. Finally, the
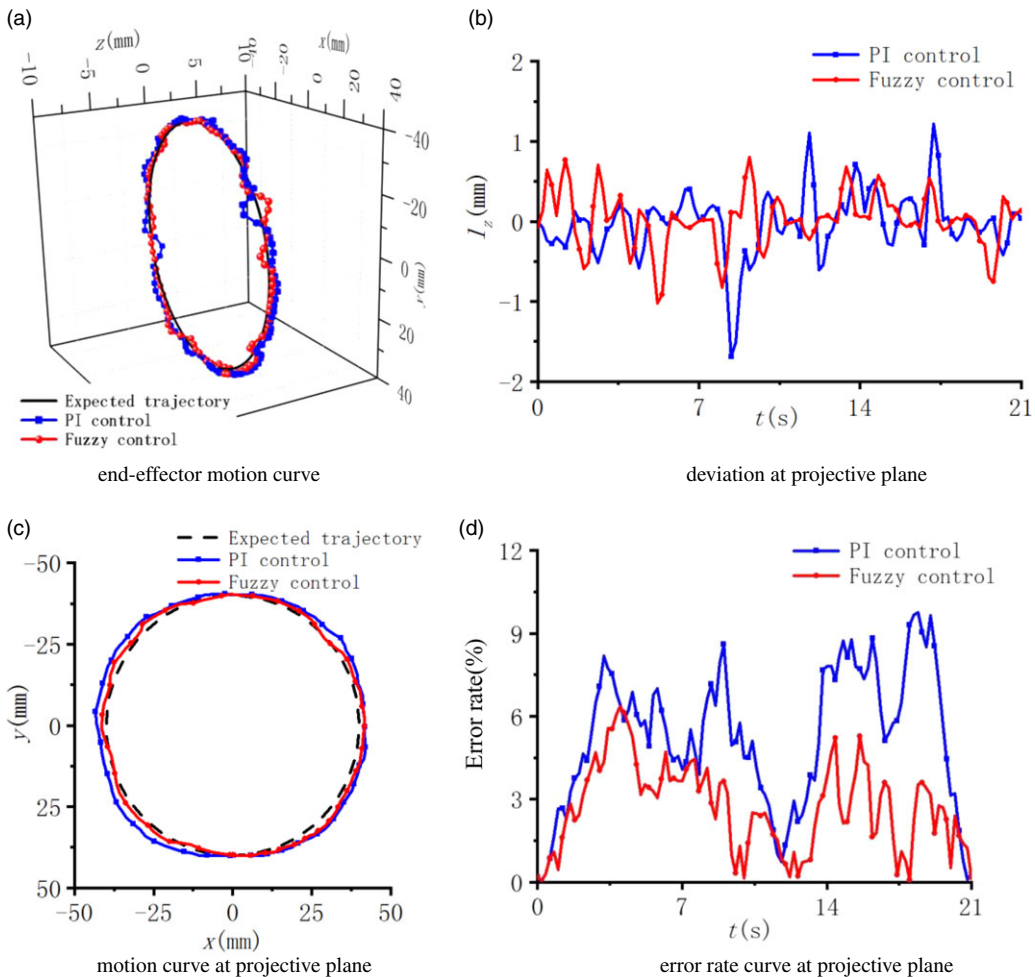
(a)

end-effector motion curve

(b)

deviation at projective plane

(c)

motion curve at projective plane

(d)

error rate curve at projective plane

Figure 14. *Experimental images of circle trajectory tracking.*

expected arc trajectory of the executive end is set as following:

$$\begin{cases} px = px_0 \\ py = py_0 + R\cos(wt) \\ pz = pz_0 + R\sin(wt) \end{cases} \tag{17}$$

In this formula, $px_0, py_0,$ and pz_0 are the initial positions of executive end of the flexible manipulator at the terminate frame. The radius of the arc is 40 mm, and the motion period is 21 s. The control parameters (K_p, K_i, K_r) are consistent with the simulation.

Note that there are some errors between the actual flexible manipulator and simulation model such as assembly errors, joint frictions, and system modeling errors that cannot be estimated precisely, meaning that the actual control of the executive end of the flexible manipulator has a little deviation from the ideal condition. The observed curves of joints' angles had slightly higher errors than simulated curves (Fig. 11).

With respect to scapula joint, tracking error range of PI robust sliding mode control for α_1, β_1, and γ_1 were $(-0.927, 0.289)$, $(-0.444, 0.310)$ and $(-0.210, 0.308)$ respectively. By contrast, tracking error range of fuzzy sliding mode control are $(-0.364, 0.333)$, $(-0.273, 0.227)$, and $(-0.065, 0.176)$, respectively. The tracking error range was reduced by 42.9%, 33.7%, and 53.5%, respectively, as shown in

Table V. *Errors of circle trajectory tracking.*

Trajectory	Deviation range	Average deviation	Max error	Average error
PI control	−1.690–1.217 mm	0.276 mm	9.748%	5.266%
Fuzzy control	−1.023–0.804 mm	0.208 mm	6.350%	2.713%
△	−37%	−25%	−35%	−48%

Table III. With respect to humerus joint, tracking error range of PI robust sliding mode control for α_2, β_2, and γ_2 were $(-0.182, 0.280)$, $(-0.477, 0.564)$, and $(-0.745, 0.667)$ respectively. By contrast, tracking error range of fuzzy sliding mode control were $(-0.106, 0.124)$, $(-0.378, 0.377)$, and $(-0.431, 0.263)$ respectively. The tracking error range was reduced by 50.2%, 27.5%, and 50.8%, respectively, as shown in Table IV. These data indicate that the trajectory of joint angle under fuzzy sliding mode control is closer to the expected curve, and the tracking error is smaller than that under PI robust sliding mode control. Fuzzy sliding mode control can better realize the joint trajectory tracking control of the flexible manipulator and has higher accuracy.

During the experiment, the control force under two sliding model control strategies was recorded. Then we got the experimental curves of the control force of the pneumatic muscles of each root of the scapula and humerus joints. As can be seen from Figs. 12 and 13, the control force of each root pneumatic artificial muscle under fuzzy sliding mode control was relatively smooth, and the high-frequency shaking was effectively controlled.

4.2. Deviation analysis of the trajectory curve

The spatial trajectory of the executive end of the manipulator is processed by the angle data collected by the sensor, and the tracking curve of the terminal trajectory is obtained. Fig. 14(a) shows the motion curve of the executive end of the flexible manipulator, Fig. 14(b) shows the curve of the deviation distance from the projection plane against time, Fig. 14(c) shows the motion curve of the spatial motion curve projected into the projection plane, and Fig. 14(d) shows the deviation error curve of the motion curve on the projection plane. The error calculation formula is shown as following:

$$\varepsilon_e = \left| \sqrt{py^2 + pz^2} - R \right| /R \tag{18}$$

According to Fig. 14(a) and (c), the flexible manipulator can make a planned arc motion with a certain accuracy. Compared with PI robust sliding mode control, the tracking error of fuzzy sliding mode control is further reduced, and its trajectory is closer to the expected arc, which satisfied the requirements of control better. According to Fig. 14(b), the executive end cannot move gently and stably on the projection plane, and there is a certain amount of deviation because of the strong coupling of the flexible manipulator. In the process of motion, the deviation range of PI robust sliding mode control from the projection plane was $(-1.690 \text{ mm}, 1.217 \text{ mm})$, with an average deviation of 0.276 mm; while the deviation range of fuzzy sliding mode control from the projection plane was $(-1.023 \text{ mm}, 0.804 \text{ mm})$, with an average deviation of 0.208 mm, with a reduction of 37% and 25%, respectively. According to Fig. 14(d), the maximum error of fuzzy sliding mode control was 5.266%, and the average error was 2.713%. Compared with the maximum error of 9.748% and the average error of 5.266% in PI robust sliding mode control, the errors of fuzzy sliding mode control were reduced by 35% and 48%, respectively. The specific tracking error is shown in Table V.

5. Conclusions

In this paper, a fuzzy sliding mode control based on saturation function is proposed where the robust term of PI robust sliding model control can be adjusted adaptively and transit smoothly.

1. It can be seen from the joint angle data in experiment in Table III and IV that the tracking error range of fuzzy sliding mode control is about 40% lower than that of PI robust sliding mode control, and its joint angle curve in the experiment is closer to the expected curve.

2. According to the control force experimental data in Figs. 12 and 13, it can be seen that the control force of each PMA under fuzzy sliding mode control changes relatively smoothly.

3. It can be seen from the deviation analysis data of track curve in Fig. 14 that the average error of fuzzy sliding mode control is 48% lower than that of PI robust sliding mode control, and the error of its track curve is smaller.

All these experimental results show that fuzzy sliding mode control can improve the precision of tracking control and has better disturbance rejection performance to some extent.

References

[1] L. Zhu, X. Shi, Z. Chen, H.-T. Zhang and C.-H. Xiong, "Adaptive servomechanism of pneumatic muscle actuators with uncertainties," *IEEE Trans. Ind. Electron.* **64**(4), 3329–3337 (2017).

[2] A. Cullell, J. C. Moreno, E. Rocon, A. Forner-Cordero and J. L. Pons, "Biologically based design of an actuator system for a knee–ankle–foot orthosis," *Mech. Mach. Theory* **44**(4), 860–872 (2009).

[3] A. Hošovský, J. Piteľ, K. Židek, M. Tóthová, J. Sárosi and L. Cveticanin, "Dynamic characterization and simulation of two-link soft robot arm with pneumatic muscles," *Mech. Mach. Theory* **103**, 98–116 (2016). http://dx.doi.org/10.1016/j.mechmachtheory.2016.04.013

[4] X. Zhao, B. Zi and L. Qian, "Design, analysis, and control of a cable-driven parallel platform with a pneumatic muscle active support," *Robotica* **35**(4), 744–765 (2015).

[5] Y. Honda, F. Miyazaki and A. Nishikawa, "Control of Pneumatic Five-Fingered Robot Hand Using Antagonistic Muscle Ratio and Antagonistic Muscle Activity," *2010 3rd IEEE RAS and EMBS International Conference on Biomedical Robotics and Biomechatronics (BioRob)* (2010).

[6] K. Liu, Y. Wu, T. Zhu, Y. Chen, Y. Lu and D. Zhao, "Improved RBF network torque control in flexible manipulator actuated by PMAs," *Robotica* **37**(2), 264–280 (2018).

[7] X. Zhu, G. Tao, B. Yao and J. Cao, "Adaptive robust posture control of a parallel manipulator driven by pneumatic muscles," *Automatica* **44**(9), 2248–2257 (2008).

[8] D. X. Ba and K. K. Ahn, "Indirect sliding mode control based on gray-box identification method for pneumatic artificial muscle," *Mechatronics* **32**, 1–11 (2015). https://doi.org/10.1016/j.mechatronics.2015.09.005

[9] K. K. Ahn and H. P. H. Anh, "Design and implementation of an adaptive recurrent neural networks (ARNN) controller of the pneumatic artificial muscle (PAM) manipulator," *Mechatronics* **19**(6), 816–828 (2009).

[10] F. Amato, D. Colacino, C. Cosentino and A. Merola, "Robust and Optimal Tracking Control for Manipulator Arm Driven by Pneumatic Muscle Actuators," *2013 IEEE International Conference on Mechatronics (ICM)* (2013) pp. 827–834.

[11] S. Xie, J. Mei, H. Liu and Y. Wang, "Hysteresis modeling and trajectory tracking control of the pneumatic muscle actuator using modified Prandtl–Ishlinskii model," *Mech. Mach. Theory* **120**, 213–224 (2018). https://doi.org/10.1177/1729881418773204

[12] J. Zhang, E. Merced, N. Sepúlveda and X. Tan, "Optimal compression of generalized Prandtl–Ishlinskii hysteresis models," *Automatica* **57**, 170–179 (2015). https://doi.org/10.1016/j.automatica.2015.04.012

[13] B. Gu, K. Liu and T. Ma, "Application of BP neural networks in force prediction of pneumatic muscle actuators," *China Meas. Testing Technol.* **41**(12), 115–118 (2015).

[14] H. P. H. Anh, C. V. Kien, N. N. Son and N. T. Nam, "New approach of sliding mode control for nonlinear uncertain pneumatic artificial muscle manipulator enhanced with adaptive fuzzy estimator," *Int. J. Adv. Rob. Syst.* **15**(3), 172988141877320 (2018).